

Mitigating the bending losses of the silica-titania-based rib waveguide structure

Muhammad Shahbaz , Łukasz Kozłowski, Muhammad A. Butt* , Ryszard Piramidowicz 

Institute of Microelectronics and Optoelectronics, Warsaw University of Technology, Koszykowa 75, 00-662 Warszawa, Poland

Article info

Article history:

Received 22 Dec. 2022

Received in revised form 09 Mar. 2023

Accepted 11 Mar. 2023

Available on-line 31 Mar. 2023

Keywords:

Photonic integrated chips;
waveguides; silica-titania; ridge
waveguide; strip waveguide.

Abstract

Optical waveguides (WGs) are widely used as interconnects in integrated optical circuits both for telecommunication and sensing applications. There are different kind of optical WG designs that offers different guiding parameters, opening a vast number of possibilities. A silica-titania ($\text{SiO}_2\text{:TiO}_2$) rib WG is discussed and examined by a numerical analysis in this article with a great emphasis on the analysis of bending losses and optimization. A modal analysis for different basic parameters of the WG is presented with a detailed wavelength-based modal analysis. Various potential fabrication methods are discussed, however, a sol-gel method and dip-coating deposition technique are proposed for the low-cost development of such WGs. Moreover, an approach towards minimizing the bending losses by adding an upper cladding layer on the rib WG is presented and described.

1. Introduction

Optical waveguide (WG) devices are being researched for utilization in integrated optical circuits for optical communication systems and sensing applications [1–4]. The development of thin-film technologies proved critical to the growth of the microelectronics industry, and this trend continues today in the field of optoelectronics [5–8]. Transition-metal-oxide (TMO) films are an appealing material for use in optoelectronics [9–11] because their substantial optical energy band gaps result in good transmission characteristics in the visible-near infrared (VIS-NIR) spectral range [12–15]. High-refractive-index TMO films and low-refractive-index silica films (SiO_2) are employed as elements of multilayer photonic structures for various photovoltaic applications [16–19]. Low-pressure chemical vapour deposition (LPCVD) [20, 21], plasma-enhanced chemical vapour deposition (PECVD) [22, 23], metalorganic chemical vapour deposition (MOCVD) [24, 25], and sol-gel technology [9, 17, 18, 26] can all be used to obtain uniform WG films [27–30]. These films with a controlled refractive index and minimal optical losses can be developed by the processes of LPCVD, PECVD, and MOCVD; however, the production of these films takes a significant amount of time, and the technological

equipment that is required is quite expensive. In contrast, the sol-gel method is not only very effective but also does not need the use of a very expensive technological equipment. High-quality WG films can be developed using the sol-gel method and a dip-coating technique [31–34] that has a controlled refractive index and an attenuation that is comparable to that achieved from films produced using the LPCVD method [35–38]. The potential optical applications of sol-gel-obtained silica (SiO_2), titania (TiO_2), and silica-titania ($\text{SiO}_2\text{:TiO}_2$) materials have attracted a lot of attention [39–41]. In our more recent studies [42–45], the numerical analysis of $\text{SiO}_2\text{:TiO}_2$ -based WG films using the same sol-gel method and dip-coating technique and different, further discussed, fabrication processes (i.e., ICP-RIE, wet-chemical etching, and NIL) for a development of WG structures has been carried out [46–48]. Rib WG structures are a common type of WGs used in silicon-based photonic integrated circuits (PICs) for telecommunications and data communications. Previous research on bending losses in rib WGs [49–52] has focused on understanding and mitigating the loss of signal strength that occurs when light passes through a WG that has been bent or curved [53–56]. Researchers have studied various methods for reducing bending losses [57–60], including the use of different materials for the WG [61] and the optimization of the WG shape [56–59]. Some studies have also explored the use of special coatings or cladding layers to improve the

*Corresponding author at: ali.butt@pw.edu.pl

WG performance in the presence of bending [62–64]. In this work, the modal analysis of a rib WG structure based on $\text{SiO}_2:\text{TiO}_2$ material is performed. Moreover, the bending losses by covering the rib WG with an upper cladding (UC) layer of refractive index lower than the WG film and substrate are also mitigated.

2. Optical thin films deposition technique

$\text{SiO}_2:\text{TiO}_2$ thin-films developed via the sol-gel method and dip-coating technique make the new low-cost PIC technological platform [65]. $\text{SiO}_2:\text{TiO}_2$ is interesting for integrated photonics because it has a tunable refractive index range of 1.6–2.2 and can work in a spectral range from VIS to NIR [46]. In addition to this, the material, when combined with the sol-gel dip-coating method, makes it possible to produce optical interconnects that have low transmission losses [66–68].

At first, the steps involved in the deposition of a single $\text{SiO}_2:\text{TiO}_2$ WG film are explained. The deposition process is illustrated in Fig. 1.

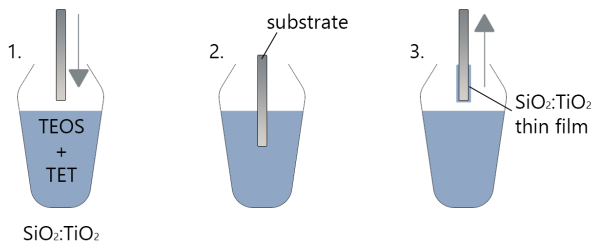


Fig. 1. Schematic representation of a sol-gel method and dip-coating technique.

To effectively use thin-film coating techniques in integrated optics, it is imperative to have precise control over the thickness of the film. This makes thickness control a crucial aspect of all thin-film development methods, including sol-gel [69, 70].

It is necessary to have the substrate and sol precursor to carry out the fabrication process. BK7 glass is favoured over other types of glass substrates because it has a lower thermal expansion coefficient and reduced surface roughness. Using the dip-coating process on BK7 glass substrates, silica-titanium WG layers were created with a $\text{SiO}_2\text{-TiO}_2$ equal to 1:1 molar ratio, which were subsequently heated to 500 °C. The primary chemical precursors for silica SiO_2 and titania TiO_2 are tetraethyl orthosilicate $\text{Si}(\text{OC}_2\text{H}_5)_4$ (TEOS) and tetraethyl orthotitanate $\text{Ti}(\text{OC}_2\text{H}_5)_4$ (TET), respectively. Water, ethanol, and hydrochloric acid (HCl), which catalyses the processes of condensation and hydrolysis, are the additional substances used in the procedure [71].

It should be emphasized that the refractive index reliance on the procedure characteristics is dependent on the stoichiometric ratio between the precursor components, and the withdrawal speed of the substrate from the sol is the primary factor determining the thickness of the deposited layer.

Previous research conducted and published by Karasiński *et al.* focused on deepening the topic of thin film fabrication [34]. By carrying out the fabrication steps carefully, the obtained thin film should be of satisfactory

parameters and could be used as an integrated photonic light guiding material.

3. Potential fabrication techniques

There are several techniques regarding the fabrication of a rib WG which depend on the WG film material, substrate, and the desired final geometry. Figure 2 shows some approaches to the production technology of $\text{SiO}_2:\text{TiO}_2$ -based optical WGs.

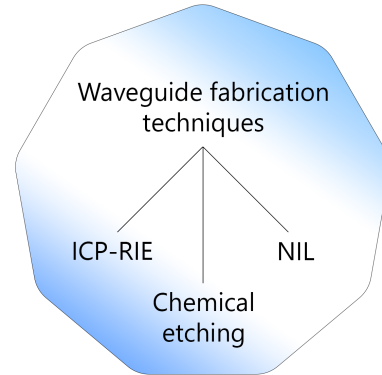


Fig. 2. Popular approaches toward WG fabrication.

The listed technologies differ in processing method and cost of production. Nevertheless, these 3 approaches are the most popular and convenient ones and should be considered when fabricating $\text{SiO}_2:\text{TiO}_2$ -based WG structures.

The most widespread and commercially available method for the development of PICs is inductively-coupled plasma-reactive ion etching (ICP-RIE). This method is mainly used in foundries and big technological facilities. The main advantage of ICP-RIE is the fact that it is well-researched and known, and it is a technology that is easy to adapt for production automation. Moreover, it provides anisotropic etching which, in the case of wet chemical etching, for example, is only achievable as isotropic etching. It also provides a good level of control over the etch rate. However, the biggest disadvantage of this technology lies in the expenses. ICP-RIE is a very expensive technology, and it requires an advanced technological facilities such as cleanroom environments. A schematic diagram of the ICP-RIE process is shown in Fig. 3 [72–75].

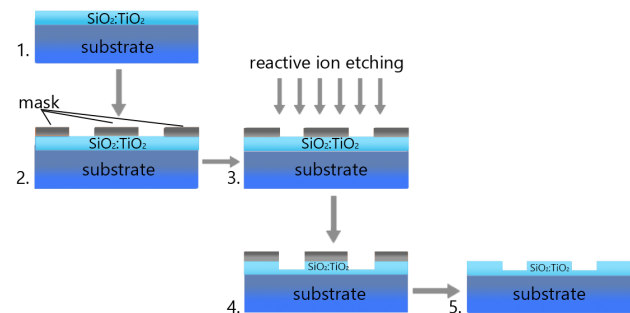


Fig. 3. Schematic representation of the RIE process. 1) Sample to be etched. 2) Photolithography to transfer the patterns on the photoresist (mask). 3) Loading the sample in the RIE chamber. 4) RIE process. 5) Removal of residual mask resulting in the final device.

Another possible approach regarding the fabrication of SiO₂:TiO₂-based optical WGs is wet chemical etching. Wet chemical etching is much more cost-efficient than ICP-RIE and is more available for a vast majority of researchers. The technological process of chemical etching is also not as complicated as other technologies.

The process of wet chemical etching is carried out in the following steps: mask deposition on the WG thin film by photolithography, chemical etching in an acid solution (e.g., HF), and finally mask removal to reveal the final WG structure. This method is especially beneficial for fabricating a small number of samples for research applications and laboratory use. However, this process is much more difficult to control and the repeatability of obtained results is not as obvious to achieve as in ICP-RIE. Also, chemical etching provides only isotropic etching which in some cases may not be desired [76]. Nevertheless, this method of fabrication gives satisfactory results [77–80].

On the other hand, rib WGs can also be fabricated by nanoimprint lithography (NIL). NIL is a simple fabrication method and has similar assets as the chemical etching technique. It is also a useful method for researchers and laboratory applications. However, it is not well-developed and widely explored for sol-gel-based materials. It is a fabrication technology with big potential regarding further development and automation. NIL could find applications in the future in foundries and big manufacturers of integrated photonics. It could be an approach that would dramatically lower the cost of production of photonic chips. The technological process of NIL stands in forming the WG structures before the hardening of the thin film. A droplet of SiO₂:TiO₂ sol-gel is deposited on the substrate and by pressing a previously prepared “master stamp”, the WG structures are transferred to the material. It is less complicated and easy to implement [47].

4. SiO₂:TiO₂ WG modal study

Figure 4 shows the graphical illustration of a rib WG structure based on a SiO₂:TiO₂ material deposited on a glass substrate, where the height of WG film is denoted as H_{film} which is fixed at 400 nm obtained via dip-coating twice with approx. 200 nm at a single dip-coating cycle. While the modal conditions are obtained by varying the width (W) and height of the rib geometry (H_{rib}) from 800 nm to 2500 nm and 50 nm to 350 nm, respectively. Practically, there are three modal regions of the optical WG which have to be explored: 1) Single-mode region: where only fundamental mode is confined. 2) Multi-mode region: where more than one mode appears due to the bigger dimensions of the WG. 3) Cut-off region: where no mode is confined due to smaller WG dimensions.

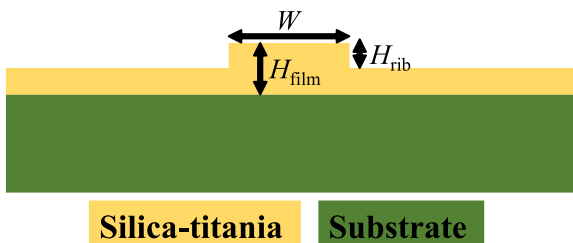


Fig. 4. Schematic representation of SiO₂:TiO₂-based rib WG.

The numerical study is performed by using the two-dimensional finite element method (2D-FEM) via commercially available COMSOL Multiphysics software. The FEM is a numerical technique used to solve partial differential equations (PDEs) and boundary value problems in engineering, physics, and other fields. It involves dividing a complex problem into smaller, simpler elements that can be individually analysed and then combined to approximate the solution to the original problem. In FEM, a large complex domain is approximated by a mesh of smaller, interconnected subdomains called finite elements. The governing equations are then applied to each element, resulting in a set of algebraic equations that can be solved for the unknowns at each node of the mesh. The method is widely used in structural mechanics, fluid dynamics, heat transfer, electromagnetic analysis, and other areas of engineering and physics. It allows for the efficient solution of complex problems that would be difficult or impossible to solve using analytical methods.

The real part of the effective refractive index [$\text{Re}(n_{\text{eff}})$] of the WG is determined for different WG dimensions which provide the information related to the number of modes confined in the specific WG geometry. The modal analysis is carried out at an operational wavelength of 1550 nm. In Fig. 5, different regions of a mode confinement can be identified. The H_{film} is constant at 400 nm throughout the paper. At $W = 800$ to 2500 nm, a flexible fundamental single-mode confinement at different values of H_{rib} can be observed, but there is no mode confinement if the values of H_{rib} are increased from 190 nm at $W = 800$ nm, 230 nm at $W = 1000$ nm, and 280 nm at $W = 1200$ nm. Furthermore, $W = 1500$ nm, 1800 nm, 2000 nm, and 2500 nm are the most flexible widths where WG stays single mode for a wide range of H_{rib} .

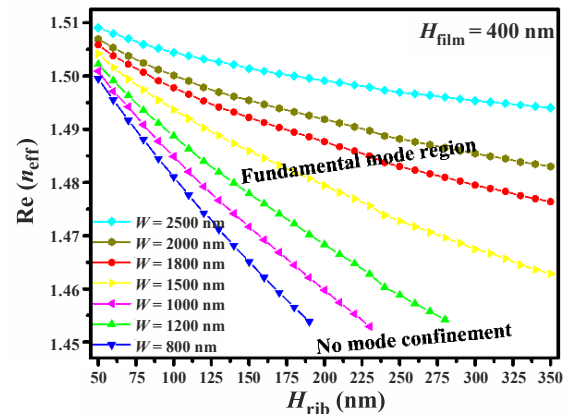


Fig. 5. Rib WG modal analysis for an operational wavelength of 1550 nm.

In Fig. 6, the regions of mode confinement for the NIR wavelength range of 1000 nm to 1600 nm are determined for a specific WG geometry. The H_{rib} and H_{film} are kept constant at 200 nm and 400 nm, respectively. For $2500 \text{ nm} \leq W \leq 1000 \text{ nm}$, the fundamental mode region is obtained for the NIR wavelength range of 1360 nm to 1600 nm, while the WG supports a multimode for the wavelengths < 1360 nm. However, for $W = 800$ nm, the single-mode region lies in the wavelength range of 1200 nm to 1520 nm. For wavelengths shorter than 1200 nm, the WG is multimode while it does not support any mode for wavelengths > 1520 nm.

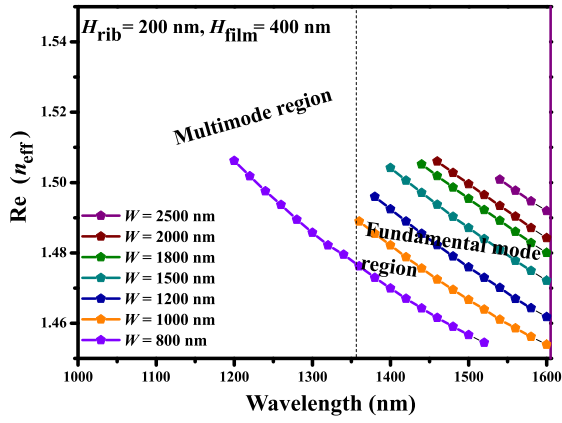


Fig. 6. Modal conditions dependent on the broad wavelength range.

The electric-field distribution in the rib WG structure at an operational wavelength of 1550 nm for $W = 2500$ nm at different H_{rib} is shown in Fig. 7(a)–(c). The single-mode conditions are quite flexible which is why the WG can only support fundamental mode at $H_{rib} = 50$ nm, 200 nm, and 350 nm as shown in Fig. 7(a), Fig. 7(b), and Fig. 7(c), respectively.

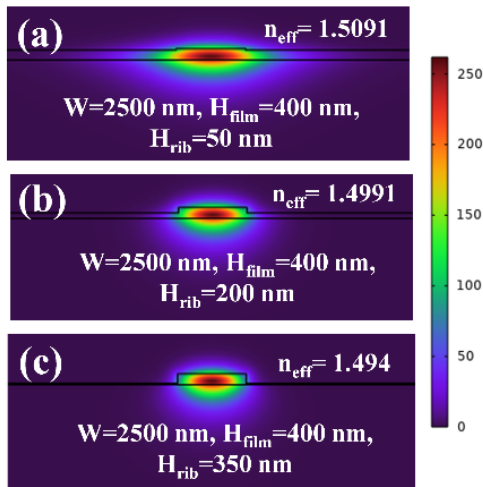


Fig. 7. Electric-field distribution in SiO₂:TiO₂-based rib WG for the operational wavelength of 1550 nm.

5. Minimizing the bending losses

When a WG is bent, the n_{eff} becomes complex, and its imaginary part is used to calculate the bend loss as follows [81]

$$2\alpha \left[\frac{dB}{turn} \right] = \frac{20}{\ln(10)} \times \frac{2\pi}{\lambda} \times \text{Im}\{n_{eff}\} \times \pi \times 2 \times R,$$

where $\text{Im}\{n_{eff}\}$ is the imaginary part of the effective refractive index, R is the bending radius in μm , and λ is the operational wavelength, i.e., 1550 nm. To reduce the bending losses of the rib WG, an UC layer of refractive index ($n = 1.3$) of height (H_{UC}) 400 nm is introduced. The suggested material for the UC layer is porous silica. It is a material that can be derived through the sol-gel method with the addition of a surface-active agent Triton X-100™ [82]. The introduction of UC at the top of the rib structure helps reduce the radius of curvature of the WG bend. As a reference point, the bending losses of the rib WG without

UC are calculated for the radius (R) of 100 μm to 500 μm as shown in Fig. 8. The WGs designed near the cut-off region can suffer from higher bending losses. That is why, the width (W) of the WG has a vital impact on the bending losses, therefore, the analysis is performed for $W = 1500$ nm, 1800 nm, 2000 nm, and 2500 nm. By adding the UC of $n = 1.3$, the difference in the bending losses for R can be compared as shown in Fig. 9. It is important to note here that by reducing the radius of curvature, we also reduce the footprint of the optical WG which is vital in the development of nano-optical devices. Some bending losses for $R = 260$ μm and varying W are shown in Table 1.

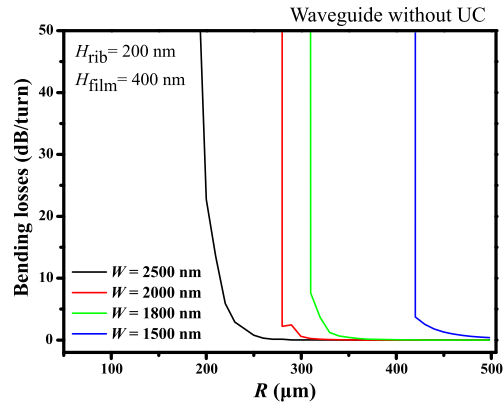


Fig. 8. Bending losses depending on the radius of curvature for a WG without the UC layer.

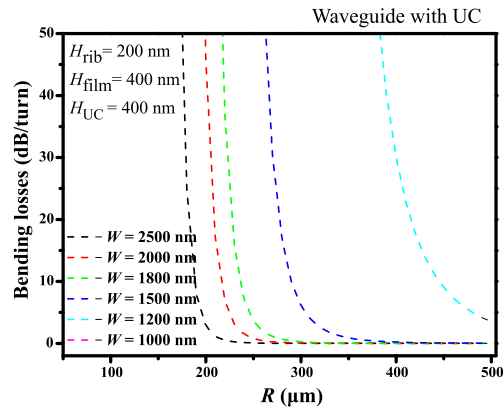


Fig. 9. Bending losses depending on the radius of curvature for a WG with the UC layer.

Table 1. Bending losses for a WG with and without UCs.

Bending losses of a WG with UC		
R [μm]	W [nm]	Bending losses [$\frac{dB}{turn}$]
260	2500	0.038
260	2000	0.43
260	1800	1.93
260	1500	> 50
Bending losses of a WG without UC		
R [μm]	W [nm]	Bending losses [$\frac{dB}{turn}$]
260	2500	0.302
260	2000	leaky
260	1800	leaky
260	1500	leaky

Finally, the E-field power distribution for the mode within the SiO₂:TiO₂-based rib WG has been considered. When studying the shape of the mode propagating inside the WG, it can be said that the majority of the E-field power resides in the core of the WG, whereas the remaining power is distributed in the substrate and the cladding region. This mainly depends on the optical properties of the material and the geometry of the WG structure. It is the natural behaviour of light propagating inside a WG. The effect can be observed when looking at the E-field distribution in Fig. 10. However, by introducing the previously mentioned additional UC layer, the mode is pulled up towards the UC. It happens due to the reduction of the contrast of refractive indices between the WG film and UC layer. In Fig. 10, the numerical analysis of the E-field distribution ratio is presented, detailing the amount of light traveling inside WG and within the substrate.

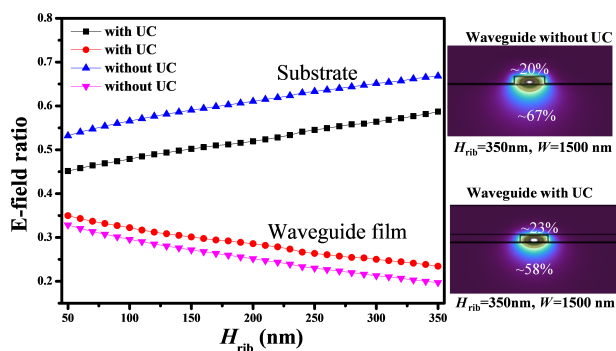


Fig. 10. E-field power distribution within the structure.

The difference between the results obtained for a WG structure with and without an UC layer tends to show a regular relationship regardless of the H_{rib} . In Fig. 10, the E-field distribution for the dimensions of $H_{\text{rib}} = 350$ nm and $W = 1500$ nm is shown for the WG structure with and without UC. In the case of WG without the UC layer, the amount of light inside the WC core is around 20% while within the substrate it is around 67%. When the UC has been applied, the results changed to ~23% inside the WG and ~58% within the substrate. The increase in the mode power inside the WG core and the reduction of mode leakage in the substrate might be one of the reasons why the application of the UC leads to lower bending losses.

6. Conclusions

Herein, a modal analysis of SiO₂:TiO₂-based rib WG is proposed to determine the single-mode, multi-mode and cut-off region of the structure. The study is conducted via the FEM. The high-quality SiO₂:TiO₂ WG films can be developed with the help of the sol-gel method and dip-coating technique. The final processing of the WG structures can be obtained via RIE. The small radius of curvature of bent WGs is important for the implementation of photonic devices with a small footprint. That is why the bending losses of the WGs should be low for a small bending radius. Here, we have suggested using an UC layer of porous silica which significantly reduces bending losses of the rib WG compared to the WG structures without an UC layer.

Acknowledgements

The research is financed by the Foundation for Polish Science from the European Regional Development Fund within the project POIR.04.04.00-00-14D6/18 "Hybrid sensor platforms for integrated photonic systems based on ceramic and polymer materials (HYPha)" (TEAM-NET program).

References

- [1] Wu, Y. *et al.* Applications of topological photonics in integrated photonic devices. *Adv. Opt. Mater.* **5**, 1700357 (2017). <https://doi.org/10.1002/adom.201700357>
- [2] Royon, M. *et al.* Sol-gel waveguide-based sensor for structural health monitoring on large surfaces in aerospace domain. *Aerospace* **8**, 109 (2021). <https://doi.org/10.3390/aerospace8040109>
- [3] Chen, Q., Li, L., Zheng, Q., Zhang, Y. & Wen, L. On-chip readout plasmonic mid-IR gas sensor. *Opto-Electron. Adv.* **3**, 190040 (2020). <https://doi.org/10.29026/oea.2020.190040>
- [4] Alberti, S. & Jágerská, J. Sol-gel thin film processing for integrated waveguide sensors. *Front. Mater.* **8**, 629822 (2021). <https://doi.org/10.3389/fmats.2021.629822>
- [5] Vlasov, Y. A. Silicon CMOS-integrated nano-photonics for computer and data communications beyond 100G. *IEEE Commun. Mag.* **50**, S67–S72 (2012). <https://doi.org/10.1109/MCOM.2012.6146487>
- [6] Dai, D. X. & Wang, S. P. Asymmetric directional couplers based on silicon nanophotonic waveguides and applications. *Front. Optoelectron.* **9**, 450–465 (2016). <https://doi.org/10.1007/s12200-016-0557-8>
- [7] Martens, D. *et al.* A low-cost integrated biosensing platform based on SiN nanophotonics for biomarker detection in urine. *Anal. Methods* **10**, 3066–3073 (2018). <https://doi.org/10.1039/c8ay00666k>
- [8] Wang, Z. *et al.* Single-shot on-chip spectral sensors based on photonic crystal slabs. *Nat. Commun.* **10**, 1–6 (2019). <https://doi.org/10.1038/s41467-019-08994-5>
- [9] Boratto, M. H., Congiu, M., dos Santos, S. B. O. & Scalvi, L. V. A. Annealing temperature influence on sol-gel processed zirconium oxide thin films for electronic applications. *Ceram. Int.* **44**, 10790–10796 (2018). <https://doi.org/10.1016/j.ceramint.2018.03.117>
- [10] Kailasa Ganapathi, S. *et al.* Highly sensitive NO₂ sensor based on ZnO nanostructured thin film prepared by SILAR technique. *Sens. Actuators B Chem.* **335**, 129678 (2021). <https://doi.org/10.1016/j.snb.2021.129678>
- [11] Bright, T. J. *et al.* Infrared optical properties of amorphous and nanocrystalline Ta₂O₅ thin films. *J. Appl. Phys.* **114**, 083515 (2013). <https://doi.org/10.1063/1.4819325>
- [12] Eiamchai, P., Chindaudom, P., Pokaipisit, A. & Limsuwan, P. A spectroscopic ellipsometry study of TiO₂ thin films prepared by ion-assisted electron-beam evaporation. *Curr. Appl. Phys.* **9**, 707–712 (2009). <https://doi.org/10.1016/j.cap.2008.06.011>
- [13] Luo, X. *et al.* Investigation of HfO₂ thin films on Si by X-ray photoelectron spectroscopy, rutherford backscattering, grazing incidence X-ray diffraction and variable angle spectroscopic ellipsometry. *Crystals* **8**, 248 (2018). <https://doi.org/10.3390/cryst8060248>
- [14] Venkataraj, S. *et al.* Structural and optical properties of thin zirconium oxide films prepared by reactive direct current magnetron sputtering. *J. Appl. Phys.* **92**, 3599–3607 (2002). <https://doi.org/10.1063/1.1503858>
- [15] Fadel, M., Azim, M., Omer, O. A. & Basily, R. R. A study of some optical properties of hafnium dioxide (HfO₂) thin films and their applications. *Appl. Phys. A* **66**, 335–343 (1998). <https://doi.org/10.1007/s003390050675>
- [16] Chee, K. W. A., Tang, Z., Lü, H. & Huang, F. Anti-reflective structures for photovoltaics: Numerical and experimental design. *Energy Rep.* **4**, 266–273 (2018). <https://doi.org/10.1016/j.egy.2018.02.002>
- [17] Gondek, E. & Karasinski, P. High reflectance materials for photovoltaics applications: Analysis and modelling. *J. Mater. Sci. Mater. Electron.* **24**, 2934–2943 (2013). <https://doi.org/10.1007/s10854-013-1194-2>
- [18] Skolik, M., Domanowska, A., Karasinski, P., Gondek, E. & Michalewicz, A. Double layer sol-gel derived antireflective coatings

- on silicon—design, optical and Auger electron spectroscopy characterization. *Mater. Lett.* **251**, 210–213 (2019). <https://doi.org/10.1016/j.matlet.2019.05.071>
- [19] Shen, H., Wang, Z., Wu, Y. & Yang, B. One-dimensional photonic crystals: Fabrication, responsiveness and emerging applications in 3D construction. *RSC Adv.* **6**, 4505–4520 (2016). <https://doi.org/10.1039/C5RA21373H>
- [20] Daldosso, N. *et al.* Comparison among various Si/sub 3N/sub 4/waveguide geometries grown within a CMOS fabrication pilot line. *J. Light. Technol.* **22**, 1734–1740 (2004). <https://doi.org/10.1109/JLT.2004.831182>
- [21] Lambeck, P. V., Van Lith, J. & Hoekstra, H. J. W.M. Three novel integrated optical sensing structures for the chemical domain. *Sens. Actuators B Chem.* **113**, 718–729 (2006). <https://doi.org/10.1016/j.snb.2005.07.024>
- [22] Gorecki, Ch. Optimization of plasma-deposited silicon oxynitride films for optical channel waveguides. *Opt. Lasers Eng.* **33**, 15–20 (2000). [https://doi.org/10.1016/S0143-8166\(00\)00024-5](https://doi.org/10.1016/S0143-8166(00)00024-5)
- [23] Wörhoff, K. A. *et al.* Plasma enhanced chemical vapor deposition silicon oxynitride optimized for application in integrated optics. *Sens. Actuators A Phys.* **74**, 9–12 (1999). [https://doi.org/10.1016/S0924-4247\(98\)00325-2](https://doi.org/10.1016/S0924-4247(98)00325-2)
- [24] Tan, S. T. *et al.* Blueshift of optical band gap in ZnO thin films grown by metal-organic chemical-vapor deposition. *J. Appl. Phys.* **98**, 013505 (2005). <https://doi.org/10.1063/1.1940137>
- [25] Pan, X. H. *et al.* Electrical and optical properties of phosphorus-doped p-type ZnO films grown by metalorganic chemical vapor deposition. *J. Appl. Phys.* **103**, 023708 (2008). <https://doi.org/10.1063/1.2828017>
- [26] Touam, T. *et al.* Low loss sol-gel TiO₂ thin films for waveguiding applications. *Coatings* **3**, 49–58 (2013). <https://doi.org/10.3390/coatings3010049>
- [27] Zaręba-Grodź, I. *et al.* Europium-doped silica–titania thin films obtained by the sol–gel method. *Opt. Mater.* **29**, 1103–1106 (2007). <https://doi.org/10.1016/j.optmat.2006.05.001>
- [28] Ferrari, J. L., de O. Lima, K. & Gonçalves, R. R. Refractive indexes and spectroscopic properties to design Er³⁺-doped SiO₂–Ta₂O₅ films as multifunctional planar waveguide platforms for optical sensors and amplifiers. *ACS Omega* **6**, 8784–8796 (2021). <https://doi.org/10.1021/acsomega.0c05351>
- [29] Forastiere, M. A. *et al.* Strip-loaded sol-gel waveguides: design and fabrication. *Fiber Integr. Opt.* **20**, 29–43 (2001). <https://doi.org/10.1080/01468030151072976>
- [30] Urlacher, C. C. Study of erbium doped ZrO₂ waveguides elaborated by a sol–gel process. *Opt. Mater.* **12**, 19–25 (1999). [https://doi.org/10.1016/S0925-3467\(98\)00051-2](https://doi.org/10.1016/S0925-3467(98)00051-2)
- [31] Karasiński, P. Silica-titania films fabricated by sol-gel method for applications in planar photonics. *Acta Phys. Pol.* **116**, S-114–S-116 (2009). <http://przyrbwn.icm.edu.pl/APP/PDF/116/a116zs31.pdf>
- [32] Karasiński, P. & Rogoziński, R. Rib waveguides fabricated by means of chemical etching of sol–gel SiO₂:TiO₂ films. *Opt. Commun.* **245**, 237–242 (2005). <https://doi.org/10.1016/j.optcom.2004.10.074>
- [33] Karasiński, P., Tyszkiewicz, C., Domanowska, A., Michalewicz, A. & Mazur, J. Low loss, long time stable sol-gel derived silica-titania waveguide films. *Mater. Lett.* **143**, 5–7 (2015). <https://doi.org/10.1016/j.matlet.2014.12.048>
- [34] Karasiński, P., Tyszkiewicz, C., Piramidowicz, R. & Kazmierczak, A. Development of integrated photonics based on SiO₂:TiO₂ sol-gel derived waveguide layers: state of the art, perspectives, prospective applications. *Proc. SPIE* **11364**, 1136414 (2020). <https://doi.org/10.1117/12.2559059>
- [35] Lukowiak, A., Dylewicz, R., Patela, S., Strek, W. & Maruszewski, K. Optical properties of SiO₂-TiO₂ thin film waveguides obtained by the sol-gel method and their applications for sensing purposes. *Opt. Mater.* **27**, 1501–1505 (2005). <https://doi.org/10.1016/j.optmat.2005.01.007>
- [36] Zięba, M. *et al.* High refractive index silica-titania films fabricated via the sol–gel method and dip-coating technique—physical and chemical characterization. *Materials* **14**, 7125 (2021). <https://doi.org/10.3390/ma14237125>
- [37] Jaglarz, J., Dulian, P. & Karasiński, P. Thermo-optical properties of porous silica thin films produced by sol-gel method. *Mater. Chem. Phys.* **243**, 122603 (2020). <https://doi.org/10.1016/j.matchemphys.2019.122603>
- [38] Nizioł, J., Gondek, E. & Karasiński, P. Changes in optical parameters of SiO₂:TiO₂ films obtained by sol-gel method observed as a result of thermal treatment. *Materials* **14**, 2290 (2021). <https://doi.org/10.3390/ma14092290>
- [39] Karasiński, P. *et al.* Highly sensitive sensor structure based on sol-gel waveguide films and grating couplers. *Electronics* **10**, 1389 (2021). <https://doi.org/10.3390/electronics10121389>
- [40] Zięba, M. *et al.* Erbium-doped sol-gel derived silica-titania films. *Proc. SPIE* **12148**, 1214803 (2022). <https://doi.org/10.1117/12.2622299>
- [41] Karasiński, P. Sol-Gel derived silica-titania waveguide films for applications in evanescent wave sensors—comprehensive study. *Materials* **15**, 7641 (2022). <https://doi.org/10.3390/ma15217641>
- [42] Kozłowski, Ł. *et al.* Low-cost integrated photonic platform developed via a sol-gel dip-coating method: A brief review. *Sens. Transducers J.* **259**, 82–92 (2022). https://sensorsportal.com/HTML/DIGEST/P_3284.htm
- [43] Butt, M. A. *et al.* Optical Waveguides For Integrated Photonics: Mainstream Technologies versus Low-Cost Silica-Titania Sol-Gel Approach Optical Waveguides For Integrated Photonics: Mainstream Technologies Versus Low-Cost Silica-Titania Sol-Gel Approach. in *Advances in Sensors: Reviews 8* (ed. Yurish, S. Y.) 85–108 (IFSA, 2022).
- [44] Kozłowski, Ł., Kaźmierczak, A., Butt, M. A. & Piramidowicz, R. Waveguide Structures Based On A Low-Cost Silica-Titania Optical Platform For Sensing Applications. *Warsaw University of Technology* (2022). <https://atam.port.org.pl/wp-content/uploads/2022/09/kozłowski-poster-online.pdf>
- [45] Butt, M. A., Tyszkiewicz, C., Karasiński, P. & Piramidowicz, R. Optical thin films fabrication techniques-towards a low-cost solution for the integrated photonic platform: a review of the current status. *Materials* **15**, 4591 (2022). <https://doi.org/10.3390/ma15134591>
- [46] Butt, M. A. Subwavelength grating waveguide structures proposed on the low-cost silica-titania platform for optical filtering and refractive index. *Int. J. Mol. Sci.* **23**, 6614 (2022). <https://doi.org/10.3390/ijms23126614>
- [47] Butt, M. A. Development of a low-cost silica-titania optical platform for integrated photonics applications. *Opt. Express* **30**, 23677–23694 (2022). <https://doi.org/10.1364/OE.460318>
- [48] Butt, M. A., Kaźmierczak, A., Tyszkiewicz, C., Karasiński, P. & Piramidowicz, R. (2021). Mode sensitivity exploration of silica-titania waveguide for refractive index sensing applications. *Sensors* **21**, 7452 (2020). <https://doi.org/10.3390/s21227452>
- [49] Brimont, A. *et al.* Low-loss and compact silicon rib waveguide bends. *IEEE Photonics Technol. Lett.* **28**, 299–302 (2015). <http://doi.org/10.1109/LPT.2015.2495230>
- [50] Dullo, F. T., Tinguely, J.-C., Stian, A. S. & Hellesø, O. G. Single-mode limit and bending losses for shallow rib Si₃N₄ waveguides. *IEEE Photon. J.* **7**, 1–11 (2015). <https://doi.org/10.1109/JPHOT.2014.2387252>
- [51] Dai, D. & He, S. Analysis of characteristics of bent rib waveguides. *J. Opt. Soc. Am. A* **21**, 113–121 (2004). <https://doi.org/10.1364/JOSAA.21.000113>
- [52] Selvaraja, S. K., Bogaerts, W., Absil, P., Van Thourhout, D. & Baets, R. Record low-loss hybrid rib/wire waveguides for silicon photonic circuits. *Group IV Photonics, Ghent University* (2010). http://www.photonics.intec.ugent.be/download/pub_2650.pdf
- [53] Butt, M. A., Khonina, S. N., Kazanskiy, N. L. Optical elements based on silicon photonics. *J. Comput. Opt.* **43**, 1079–1083 (2019). <https://computeroptics.ru/eng/KO/Annot/KO43-6/430618e.html>
- [54] Bogaerts, W. & Selvaraja, S. K. Compact single-mode silicon hybrid rib/strip waveguide with adiabatic bends. *IEEE Photon. J.* **3**, 422–432 (2011). <https://doi.org/10.1109/JPHOT.2011.2142931>
- [55] Pennings, E. C. M. & Deri, R. J. Simple Method For Estimating Useable Bend Radii Of Deeply Etched Optical Rib Waveguides. in *Integrated Photonics Research* paper ThF1 (Optica Publishing Group, 1991). <https://doi.org/10.1364/IPR.1991.ThF1>
- [56] Seo, Ch. & Chen, J. C. Low transition losses in bent rib waveguides. *J. Light. Technol.* **14**, 2255–2259 (1996). <https://doi.org/10.1109/50.541216>
- [57] Rahman, B. M. A. Leung, D. M. H., Obayya, S. S. A. & Grattan, K. T. V. Numerical analysis of bent waveguides: bending loss, transmission loss, mode coupling, and polarization coupling. *Appl. Opt.* **47**, 2961–2970 (2008). <https://doi.org/10.1364/AO.47.002961>

- [58] Chen, Y., Yu, J., Yan, Q. & Chen, S. Analysis on influencing factors of bend loss of silicon-on-insulator waveguides. *Chin. J. Semicond.* **26**, 216–219 (2005). <http://www.jos.ac.cn/en/article/id/481c837e-a5a4-4e55-85f4-968472367b5b>
- [59] Nurdiani, Z. & Ehsan, A. A. Large cross-section rib silicon-on-insulator (SOI) S-bend waveguide. *Optik* **130**, 1414–1420 (2017). <https://doi.org/10.1016/j.ijleo.2016.11.161>
- [60] Srinivasan, H., Bommalakunta, B., Chamberlain, A. & Hastings, J. T. Finite element analysis and experimental verification of SOI waveguide bending loss. *Microw. Opt. Technol. Lett.* **51**, 699–702 (2009). <https://doi.org/10.1002/mop.24135>
- [61] Austin, M. & Flavin, P. Small-radii curved rib waveguides in GaAs/GaAlAs using electron-beam lithography. *J. Light. Technol.* **1**, 236–240 (1983). <https://doi.org/10.1109/JLT.1983.1072088>
- [62] Galarza, M. *et al.* Simple low-loss waveguide bends using ARROW effect. *Appl. Phys. B* **80**, 745–748 (2005). <https://doi.org/10.1007/s00340-005-1775-8>
- [63] Subramaniam, V., De Brabander, G. N., Naghski, D. H. & Boyd, J. T. Measurement of mode field profiles and bending and transition losses in curved optical channel waveguides. *J. Light. Technol.* **15**, 990–997 (1997). <https://doi.org/10.1109/50.588672>
- [64] Pandraud, G., French, P. J. & Sarro, P. M. Experimental study of bent SiC optical waveguides. *Microw. Opt. Technol. Lett.* **47**, 219–220 (2005). <https://doi.org/10.1002/mop.21128>
- [65] Golonka, L. *et al.* Low temperature co-fired ceramics (LTCC) microsystems. *Opt. Appl.* **41**, 383–388 (2011). https://dbc.wroc.pl/Content/57700/PDF/optappl_4102p383.pdf
- [66] Vasconcelos, H. C. Optical Waveguides Based On Sol-Gel Coatings. in *Electromagnetic Propagation and Waveguides in Photonics and Microwave Engineering* (ed. Steglich, P.) Ch. 3 (IntechOpen, 2020). <https://doi.org/10.5772/intechopen.91993>
- [67] Nowak, K. *et al.* Sol-Gel-Based Optical Waveguides On LTCC Substrates. in *31st International Spring Seminar on Electronics Technology* 518–522 (IEEE, 2008). <https://doi.org/10.1109/ISSE.2008.5276621>
- [68] Tadaszak, R. J., Łukowiak, A., Golonka, L. J. & Patela, S. Hybrid sol–gel–glaze planar optical waveguides on LTCC substrate—preliminary works. *Opt. Appl.* **41**, 493–500 (2011).
- [69] Butt, M. A. Thin-film coating methods: a successful marriage of high-quality and cost-effectiveness—a brief exploration. *Coatings* **12**, 1115 (2022). <https://doi.org/10.3390/coatings12081115>
- [70] Karasiński, P. Sol-gel derived optical waveguide films for planar sensors with phase modulation. *Opt. Appl.* **34**, 467–475 (2004). https://delibra.bg.polsl.pl/Content/28404/BCPS_32162_-_Sol-gel-derived-opti_0000.pdf
- [71] Karasiński, P., Jaglarz, J. & Mazur, J. Low loss silica-titania waveguide films. *Photonics Lett. Poland* **2**, 37–39 (2010). <https://doi.org/10.4302/plp.2010.1.13>
- [72] Lishan, D. Plasma etching: comparing PE, RIE and ICP-RIE. *Plasma-Therm* (2020). www.plasmatherm.com
- [73] Jansen, H., Gardeniers, H., de Boer, M., Elwenspoek, M. & Fluitman, J. A survey on the reactive ion etching of silicon in microtechnology. *J. Micromech. Mikroeng.* **6**, 14 (1996). <https://doi.org/10.1088/0960-1317/6/1/002>
- [74] Karasiński, P., Tyszkiewicz, C. & Rogoziński, R. Single-mode rib waveguides fabricated by means of sol-gel method. *Acta Phys. Pol.* **118**, 1168–1170 (2010). <http://przyrbwn.icm.edu.pl/APP/PDF/118/a118z6p20.pdf>
- [75] Schwartz, G. C. & Schaible, P. M. Reactive ion etching of silicon. *J. Vac. Sci. Technol.* **16**, 410–413 (1979). <https://doi.org/10.1116/1.569962>
- [76] Karasiński, P., Tyszkiewicz, C., Rogoziński, R., Jaglarz, J. & Mazur, J. Optical rib waveguides based on sol-gel derived silica-titania films. *Thin Solid Films* **519**, 5544–5551 (2011). <https://doi.org/10.1016/j.tsf.2011.02.064>
- [77] Iliescu, C. & Tay, F. E. H. Wet etching of glass. in *Proceedings of the International Semiconductor Conference CAS 1*, 35–44 (2005). <https://doi.org/10.1109/SMICND.2005.1558704>
- [78] Hyeongsik, P. *et al.* A review of wet chemical etching of glasses in hydrofluoric acid based solution for thin film silicon solar cell application. *Curr. Photovolt. Res.* **5**, 75–82 (2017). <https://doi.org/10.21218/CPR.2017.5.3.075>
- [79] Spierings, G. Wet chemical etching of silicate glasses in hydrofluoric acid based solutions. *J. Mater. Sci.* **28**, 6261–6273 (1993). <https://doi.org/10.1007/BF01352182>
- [80] Shubhava, A. *et al.* Chemical etching of glasses in hydrofluoric acid: A brief review. *Materials Today Proc.* **55**, 46–51 (2022). <https://doi.org/10.1016/j.matpr.2021.12.110>
- [81] Butt, M. A., Kozłowski, L. & Piramidowicz, R. Numerical scrutiny of a silica-titania-based reverse rib waveguide with vertical and rounded sidewalls. *Appl. Opt.* **62**, 1296–1302 (2023). <https://doi.org/10.1364/AO.480856>
- [82] Karasiński, P., Jaglarz, J., Reben, M., Skoczek, E. & Mazur, J. Porous silica xerogel films as antireflective coatings – fabrication and characterization. *Opt. Mater.* **33**, 1989–1994 (2011). <https://doi.org/10.1016/j.optmat.2011.04.003>